Characterization of a purely thermal wave based photopyroelectric gas sensor for hydrogen detection

Mahendra Munidasa, Andreas Mandelis, Arrin Katz, Do V. Do, and Viet K. Luong
Photothermal and Optoelectronic Diagnostics Laboratory, Department of Mechanical Engineering and Center for Hydrogen and Electrochemical Studies (CHES), University of Toronto, Toronto, Ontario M5S 1A4, Canada

(Received 19 August 1993; accepted for publication 16 March 1994)

A study towards the characterization of a new photopyroelectric gas sensor with an operating mechanism based purely on thermal waves is performed. It has been found that by restricting the gas flow over the sensor to a thin layer, sensitivity of the phase of the photopyroelectric signal to hydrogen is greatly enhanced. The phase of the signal has been shown to be more stable than the amplitude. Furthermore, the thinner the pyroelectric film, the better the sensitivity. Hydrogen concentrations as low as 1% in air have been detected using a 9 μm film.

In a very recent development,[1] a photopyroelectric (PPE) gas sensor based on a purely thermal wave nonchemical operating mechanism has been described and its application to hydrogen sensing has been discussed. This is in contrast with a similar, surface chemically active Pd-coated device introduced earlier.[2] In both these sensors metallized polyvinylidene fluoride (PVDF) films[3] have been used. In the new nonchemical device, sensitivity to a particular gas is obtained through thermal boundary condition changes introduced by the gas at the film–gas interface, which depend on the thermophysical properties of the gas. In this paper we describe the characteristics of this sensor with a new geometry which improved the sensitivity considerably.

A commercial PVDF film[3] with Ni/Al electrodes on both sides was installed in a commercially available INFICON™ housing [Fig. 1(a)]. Light from an intensity-modulated laser diode with variable frequency was guided on to the back of the film using an optical fiber. The sensor was placed inside a chamber which permitted the controlled continuous flow of gas over the sensor. The photopyroelectric signal from the film was preamplified and then connected to a lock-in amplifier, which was interfaced to a computer to record both amplitude and phase. A complete description of the experimental setup is given in Ref. 1. In the present improved geometry, gas flow over the PVDF film opposite to the laser side has been restricted to a thin layer smaller than the thermal diffusion length μ in the sensing gas (in this case hydrogen). The thermal diffusion length μ is given by

$$\mu=\sqrt{\frac{2\alpha}{\omega}}, \tag{1}$$

where ω is the angular modulation frequency of the laser intensity and α is the thermal diffusivity of the gas. This geometry is achieved by placing a solid plate over the detector as shown in Fig. 1(a). In our setup the gap between the plate and the surface of the film is 0.5 mm. (The thermal diffusion length in hydrogen at 11 Hz is 2.3 mm.)

This setup can be modeled as a four-layer system as shown in Fig. 1(b). Following the same approach as in Ref. 1 the pyroelectric voltage, which is proportional to the average temperature of the film for a given gas, can be calculated by solving the one-dimensional heat diffusion equations with appropriate boundary conditions, in each region (s), (b), (f), and (g) [Fig. 1(b)]. The final solution is given by

$$\tilde{T}_f(\omega)=\frac{Q_0}{Lk_f\sigma_f^2}\frac{(1+b_{bf})}{(1+b_{gf})}$$
$$=\frac{[1+\gamma_{bf}\gamma_{sb}\exp(-2\sigma_b d)+[\gamma_{bf}+\gamma_{sb}\exp(-2\sigma_b d)]\exp(-\sigma_f L)][1-\exp(-\sigma_f L)]}{(1+b_{bf})[1+\gamma_{bf}\gamma_{sb}\exp(-2\sigma_b d)][1+\gamma_{gf}\exp(-2\sigma_f L)]-2\gamma_{gf}[1+\gamma_{sb}\exp(-2\sigma_b d)]\exp(-2\sigma_f L)}, \tag{2}$$

where

$$b_{ij}=\frac{k_i\sigma_i}{k_j\sigma_j}=\frac{k_i}{k_j}\sqrt{\frac{\alpha_j}{\alpha_i}}=\frac{\sqrt{\rho_i c_i k_i}}{\sqrt{\rho_j c_j k_j}}, \tag{3}$$

$$\gamma_{ij}=\frac{1-b_{ij}}{1+b_{ij}}, \tag{4}$$

and

$$\sigma_j=(1+i)\sqrt{\frac{\omega}{2\alpha_j}} \tag{5}$$

with σ_j, c_j, α_j, and k_j being the density, specific heat, thermal diffusivity, and thermal conductivity of material j. In our experimental setup, the gases in both regions (b) and (g) are identical, which simplifies Eq. (2). Detailed calculations where regions (b) and (g) are considered different show that if hydrogen does not reach the laser side of the film [region

 0034-6748/94/65(6)/1983/5/$6.00

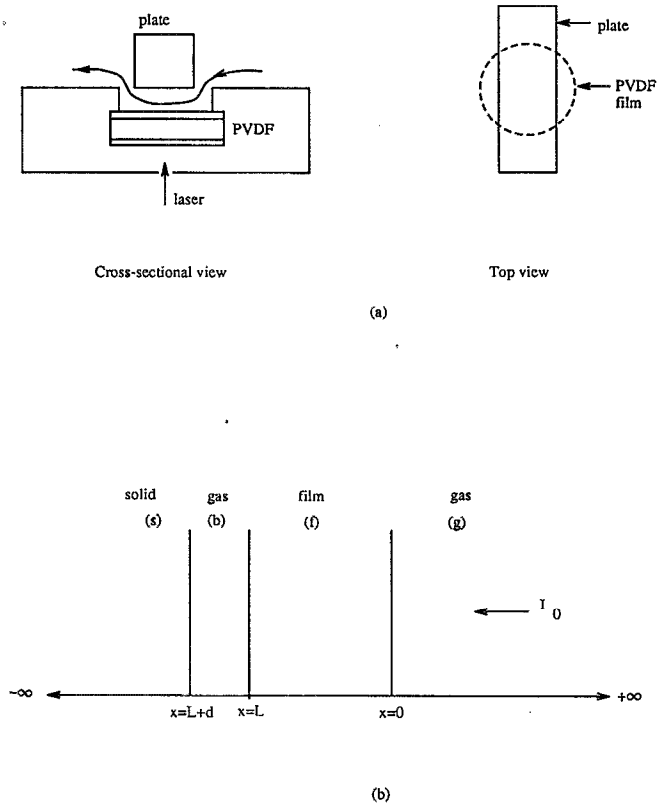

FIG. 1. (a) Cross-sectional view (left) and top view (right) of the PVDF film with the *a* plate (cap) over it. (b) Basic geometry of the sensor. PVDF film (f) of thickness L with a semi-infinite region of gas on the laser side (g) and a gas layer (b) of thickness d on the opposite side, followed by a semi-infinite region of solid (s).

(g)], which may be the case of a future miniaturized redesign of this sensor, the drop in sensitivity is insignificant. When the detector is placed in two different gases, $g1$ and $g2$ (e.g., 100% H_2 and 100% air), the amplitude ratio and the phase difference can be found by separating the real and imaginary parts of

$$\frac{\bar{T}_f(\omega;g_1)}{\bar{T}_f(\omega;g_2)}, \tag{6}$$

respectively (see appendix for details).

The theoretical behavior of the phase difference as a function of the laser modulation frequency is shown in Fig. 2 (solid line). The following thermophysical parameters have been used in calculating the curve; $k_{air}=26.14\times10^{-3}$ W m^{-1} K^{-1}, $\alpha_{air}=22.03\times10^{-6}$ m^2 s^{-1}, $k_H=182\times10^{-3}$ W m^{-1} K^{-1}, $\alpha_H=155.4\times10^{-6}$ m^2 s^{-1},[4] $k_f=190\times10^{-3}$ W m^{-1} K^{-1}, $\alpha_f=8\times10^{-8}$ m^2 s^{-1}.[3] A film of thickness 28 μm, gas layer of thickness $d=0.5$ mm, and a solid plate of glass ($k_{glass}=1.3$ W m^{-1} K^{-1} and $\alpha_{glass}=7.8\times10^{-7}$ m^2 s^{-1} from Ref. 4) has been assumed reflecting the experimental situation. Corresponding experimental phase differences at several frequencies are shown as discrete points in the same graph. The present configuration shows ~350% increase in phase difference compared to the open detector[1] at 10 Hz. In fact, the amplitude ratio becomes less sensitive to hydrogen when capped (placing a solid plate over the sensor). It can be

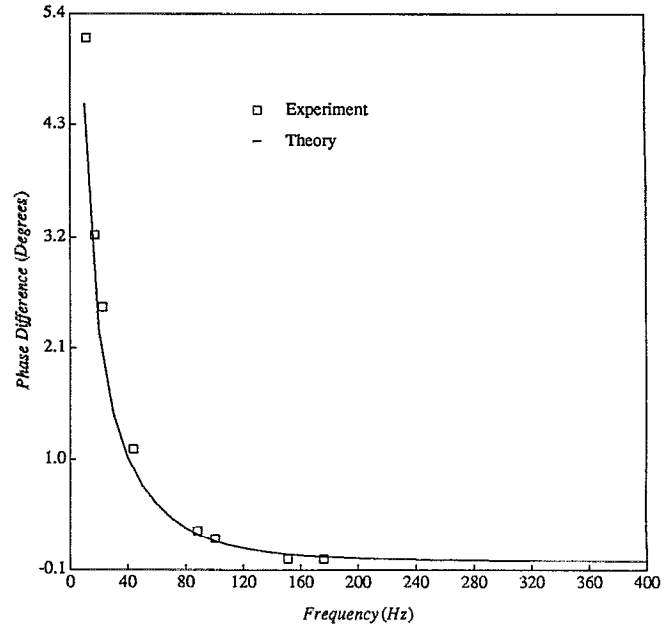

FIG. 2. Theoretical (solid line) and experimental (discrete squares) phase difference between 100% hydrogen and pure air as a function of laser modulation frequency.

shown theoretically that the phase sensitivity of the sensor to hydrogen gas with different capping materials such as aluminum, glass, and rubber changes only slightly, which is not observable experimentally. The reason is that the signal is a function of $k/(\alpha)^{1/2}$ of the capping material and is relatively insensitive to a change of less than two orders of magnitude of this quantity.

Plots of Eqs. (A14) and (A15) show that the sensitivity of the detector increases with decreasing film thickness in both amplitude and phase channels. The amplitude ratio and

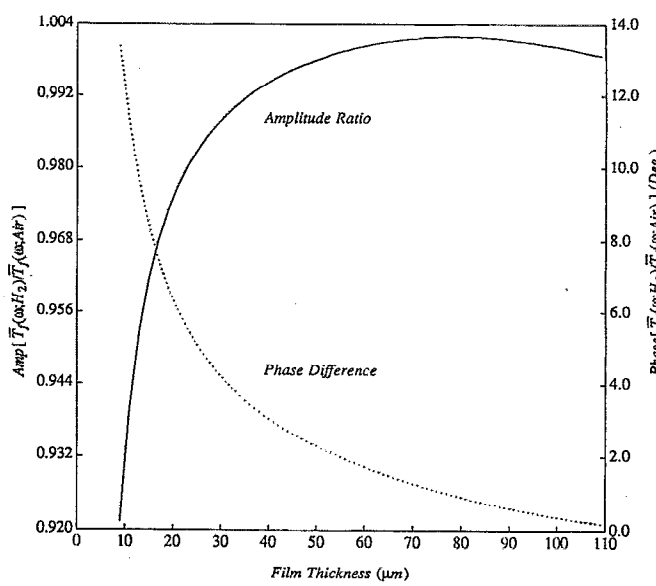

FIG. 3. Theoretically calculated amplitude ratio (solid) and phase difference (dotted) between 100% hydrogen and pure air as a function of PVDF film thickness.

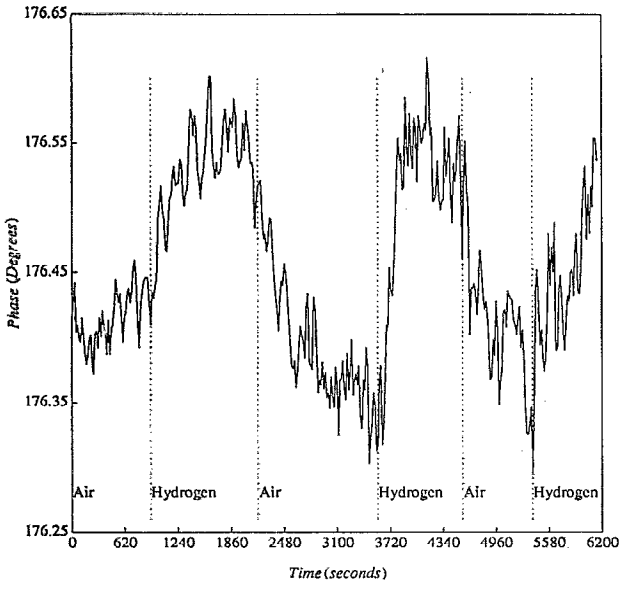

FIG. 4. The experimental phase of the PPE signal for two cycles of pure air and 1% hydrogen in air. PVDF film thickness $L=9$ μm.

the phase difference as a function of film thickness L at 10 Hz for 100% air and 100% hydrogen is shown in Fig. 3. With a 28-μm-thick PVDF film we were able to detect only down to 5% hydrogen in air, but with a 9-μm-thick film we were able to go down to 1% hydrogen in air (Fig. 4). At these low concentrations signal changes due to hydrogen were observed only in the phase channel.

Figure 5 shows data taken immediately after a new 28-μm-thick film was inserted in the housing. Several cycles of 100% hydrogen and 100% air are shown with a capped PVDF film at 21 Hz. These data show that the film responds immediately to hydrogen whereas in the Pd-PVDF chemical sensor several cycles of hydrogen exposure are required until a stabilized response is achieved. Furthermore, the phase of

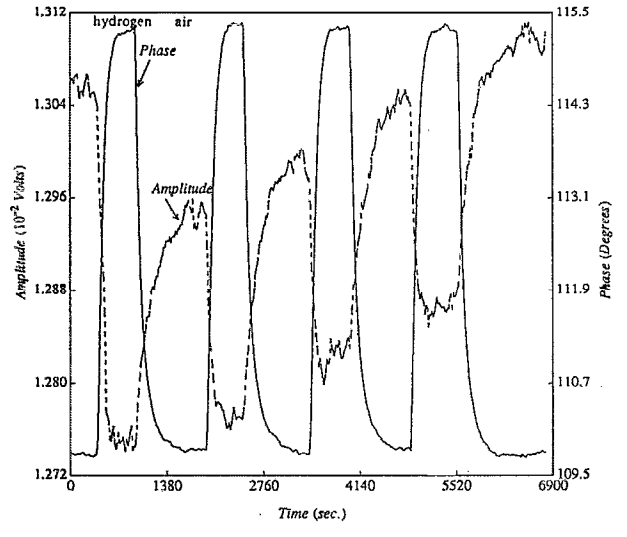

FIG. 5. The amplitude (dashed) and the phase (solid) of the PPE signal for the first four cycles of pure hydrogen and pure air immediately after inserting a fresh film of thickness 28 μm.

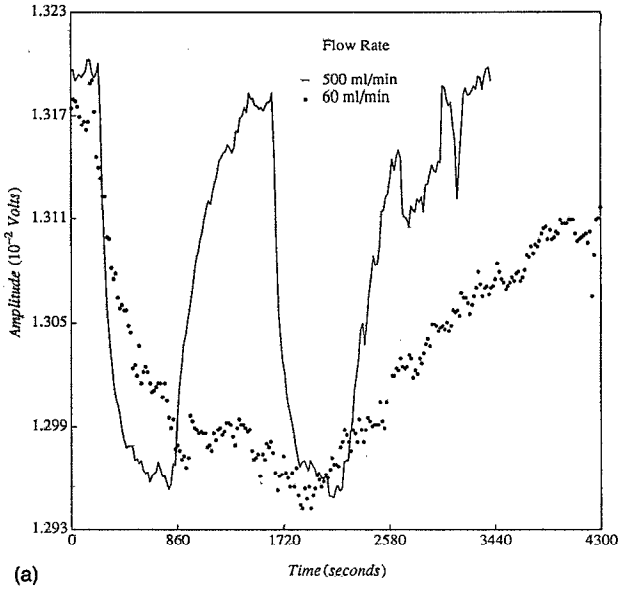

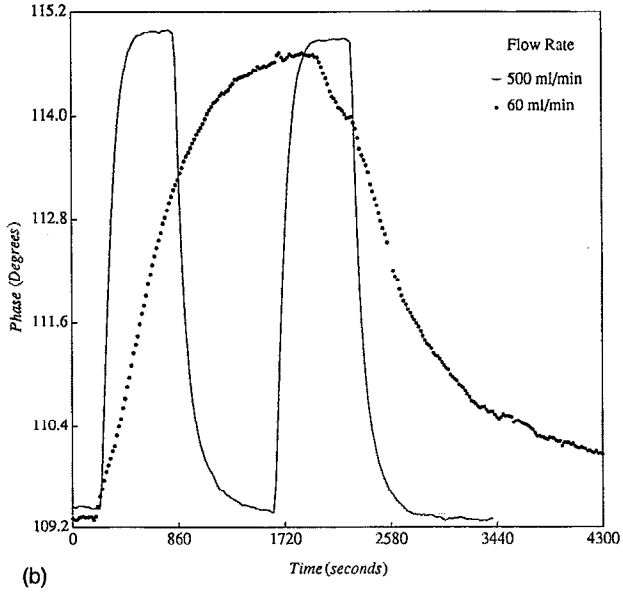

FIG. 6. Solid lines show (a) amplitude and (b) phase of the signal for two cycles of pure hydrogen and pure air at a flow rate of 500 ml/min after film exposure to the system ambient for several hours. Dotted lines show the (a) amplitude and (b) phase for one cycle of pure hydrogen and pure air at a flow rate of 60 ml/min.

the signal shows excellent quality, reproducibility, and reversibility, whereas the amplitude drifts. Figure 6 shows data taken several hours later (solid lines) where the amplitude has stabilized. Here as well the phase data look far superior and have not drifted or changed in magnitude during the idle period. This experiment was repeated after the optical fiber was disconnected from the chamber and reinserted after half an hour. The amplitude started drifting again as before. After some time the amplitude stopped drifting. This suggests that the change is due to the drift in the dc temperature of the film. For the data shown so far, the flow rate of both gases was 500 ml min^{-1}. Dotted lines in Fig. 6 show the amplitude and phase change due to 100% hydrogen relative to pure air at a flow rate of 60 ml/min. This clearly shows that the saturation level of the signal is independent of the flow rate

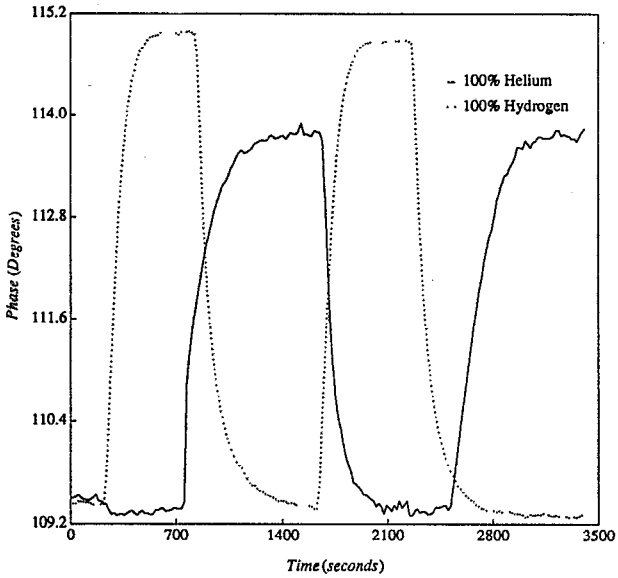

FIG. 7. The phase of the PPE signal for pure helium (solid line) and air compared with pure hydrogen (dotted line) and air.

(at least at flow rates less than 500 ml/min) and it only determines the rate at which the saturation is achieved.

As discussed in Ref. 1, this PPE sensor also shows good sensitivity to helium. Figure 7 (solid line) shows the phase of the PPE signal for 100% helium relative to pure air. The data for 100% hydrogen shown in Fig. 6(b) are repeated here for comparison. The change in phase due to helium is ~81% of the phase change due to hydrogen and Eq. (6) predicts a change of 79% ($k_{He}=152\times10^{-3}$ W m^{-1} K^{-1} and $\alpha_H=180\times10^{-6}$ m^2 s^{-1} from Ref. 4). The discrepancy may be due to the three dimensionality of the heat flow in the experiment where the optical fiber was very close to the film.

In conclusion, we have successfully demonstrated the reproducibility and the reversibility of a nonchemical photopyroelectric hydrogen gas sensor. Irreversible sensitivity loss with each successive introduction of hydrogen up to several exposures reported for Pd-based chemical sensors[5] is not present in this detector. Therefore, it is not necessary to reactivate the sensor after a prolonged idle time. Since any inexpensive metal can be used as electrodes, the cost of the sensor is greatly reduced.

We have demonstrated two ways of improving the sensitivity of the sensor; (1) by placing a cap over the film so that the gas flow over the detector is restricted to a thin layer, and (2) by using a thinner film. The data strongly suggest that the phase of the signal is the channel to be used in terms of stability. Although the sensitivity of this sensor is not as good as the Pd-based sensor, a reasonably good sensitivity of 1% hydrogen in air has been achieved. It is important to note that this concentration (1%) is not believed to be an absolute minimum. A future optimization of our setup is expected to better this level of sensitivity.

APPENDIX

Assuming both sides of the film [region (b) and (g) in Fig. 1(b)] are exposed to the same gas, the ratio of the signals in hydrogen and in air is given by

$$\frac{\tilde{T}_f(\omega;\mathrm{H_2})}{\tilde{T}_f(\omega;\mathrm{Air})}=\frac{(1+b_a)}{(1+b_h)}\frac{[\mathrm{Ren1}+\mathrm{Ren2}+i(\mathrm{Imn1}+\mathrm{Imn2})]}{[\mathrm{Red1}+\mathrm{Red2}+i(\mathrm{Imd1}+\mathrm{Imd2})]}\frac{[\mathrm{Ren3}+i\mathrm{Imn3}]}{[\mathrm{Red3}+i\mathrm{Imd3}]}, \tag{A1}$$

with the following definitions:

$$\begin{aligned}\mathrm{Ren1}=&(1+b_{af})(1+\gamma_{af}\exp(-2La_f)\cos(2La_f)\\&+\gamma_{af}\gamma_{sa}\exp(-2da_a)\cos(2da_a)+\gamma_{af}^2\gamma_{sa}\\&\times\exp[-2(da_a+La_f)]\cos(2da_a+2La_f)),\end{aligned} \tag{A2}$$

$$\begin{aligned}\mathrm{Ren2}=&2\gamma_{af}\exp(-2La_f)\cos(2La_f)-2\gamma_{af}\gamma_{sa}\\&\times\exp[-2(da_a+La_f)]\cos(2da_a+2La_f),\end{aligned} \tag{A3}$$

$$\begin{aligned}\mathrm{Imn1}=&-(1+b_{af})(\gamma_{af}\exp(-2La_f)\sin(2La_f)\\&+\gamma_{af}\gamma_{sa}\exp(-2da_a)\sin(2da_a)+\gamma_{af}^2\gamma_{sa}\\&\times\exp[-2(da_a+La_f)]\sin(2da_a+2La_f)),\end{aligned} \tag{A4}$$

$$\begin{aligned}\mathrm{Imn2}=&2\gamma_{af}[\exp(-2La_f)\sin(2La_f)+\gamma_{sa}\\&\times\exp[-2(da_a+La_f)]\sin(2da_a+2La_f)],\end{aligned} \tag{A5}$$

$$\begin{aligned}\mathrm{Red1}=&(1+b_{af})(1+\gamma_{hf}\exp(-2La_f)\cos(2La_f)\\&+\gamma_{hf}\gamma_{sh}\exp(-2da_h)\cos(2da_h)+\gamma_{hf}^2\gamma_{sh}\\&\times\exp[-2(da_h+La_f)]\cos(2da_h+2La_f)),\end{aligned} \tag{A6}$$

$$\begin{aligned}\mathrm{Red2}=&-2\gamma_{hf}[\exp(-2La_f)\cos(2La_f)+\gamma_{sh}\\&\times\exp[-2(da_h+La_f)]\cos(2da_h+2La_f)],\end{aligned} \tag{A7}$$

$$\begin{aligned}\mathrm{Imd1}=&-(1+b_{hf})[\gamma_{hf}\exp(-2La_f)\sin(2La_f)\\&+\gamma_{hf}\gamma_{sh}\exp(-2da_h)\sin(2da_h)+\gamma_{hf}^2\gamma_{sh}\\&\times\exp[-2(da_h+La_f)]\sin(2da_h+2La_f)],\end{aligned} \tag{A8}$$

$$\mathrm{Imd2}=2\gamma_{hf}\exp(-2La_f)\sin(2La_f)+2\gamma_{hf}\gamma_{sh}\times\exp[-2(da_h+La_f)]\sin(2da_h+2La_f), \quad \text{(A9)}$$

$$\mathrm{Ren3}=(1+b_{hf})(1+\gamma_{hf}\gamma_{sh}\exp(-2da_h)\cos(2da_h)+\gamma_{hf}\exp(-La_f)\cos(La_f)+\gamma_{sh}\times\exp[-2(da_h+La_f)]\cos(2da_h+La_f)), \quad \text{(A10)}$$

$$\mathrm{Red3}=(1+b_{af})(1+\gamma_{af}\gamma_{sa}\exp(-2da_a)\cos(2da_a)+\gamma_{af}\exp(-La_f)\cos(La_f)+\gamma_{sa}\times\exp[-(2da_a+La_f)]\cos(2da_a+La_f)), \quad \text{(A11)}$$

$$\mathrm{Imn3}=-(1+b_{hf})(\gamma_{hf}\gamma_{sh}\exp(-2da_h)\sin(2da_h)+\gamma_{hf}\exp(-La_f)\sin(La_f)+\gamma_{sh}\times\exp[-(2da_h+La_f)]\sin(2da_h+La_f)), \quad \text{(A12)}$$

$$\mathrm{Imd3}=-(1+b_{af})(\gamma_{af}\gamma_{sa}\exp(-2da_a)\sin(2da_a)+\gamma_{af}\exp(-La_f)\sin(La_f)+\gamma_{sa}\times\exp[-(2da_a+La_f)]\sin(2da_a+La_f)). \quad \text{(A13)}$$

Therefore, the amplitude ratio is given by

$$\frac{A_{\mathrm{H2}}(\omega)}{A_{\mathrm{air}}(\omega)}=\frac{(1+b_{af})}{(1+b_{hf})}\sqrt{\frac{(\mathrm{Ren1}+\mathrm{Ren2})^2+(\mathrm{Imn1}+\mathrm{Imn2})^2}{(\mathrm{Red1}+\mathrm{Red2})^2+(\mathrm{Imd1}+\mathrm{Imd2})^2}\cdot\frac{\mathrm{Ren3}^2+\mathrm{Imn3}^2}{\mathrm{Red3}^2+\mathrm{Imd3}^2}} \quad \text{(A14)}$$

and the phase difference is given by

$$\theta_{\mathrm{H_2}}(\omega)-\theta_{\mathrm{air}}(\omega)=\tan^{-1}\left(\frac{\mathrm{Imn1}+\mathrm{Imn2}}{\mathrm{Ren1}+\mathrm{Ren2}}\right)-\tan^{-1}\left(\frac{\mathrm{Imd1}+\mathrm{Imd2}}{\mathrm{Red1}+\mathrm{Red2}}\right)+\tan^{-1}\left(\frac{\mathrm{Imn3}}{\mathrm{Ren3}}\right)-\tan^{-1}\left(\frac{\mathrm{Imd3}}{\mathrm{Red3}}\right). \quad \text{(A15)}$$

Here subscripts a, h, f, and s stand for air, hydrogen, film, and solid cap, respectively. The quantity a_j is $1/\mu_j$ as defined in Eq. (1) for the medium j.

ACKNOWLEDGMENTS

The support of the Ministry of Energy, Mines and Resources Canada through a contract to CHES is gratefully acknowledged. We also thank Frank Ficnar for his programming efforts.

[1] M. Munidasa and A. Mandelis, Rev. Sci. Instrum. (this issue).
[2] A. Mandelis and C. Christofides, J. Appl. Phys. **70**, 4496 (1991).
[3] KYNAR Piezo Film Technical Manual, Pennwalt Corp., King of Prussia, PA (1983).
[4] J. H. Lienhard, *A Heat Transfer Textbook* (Prentice-Hall, Englewood Cliffs, NJ, 1981), pp. 495–501.
[5] C. Christofides and A. Mandelis, J. Appl. Phys. **66**, 3975 (1989).